

# Rapid lake level fall in Pangong Tso (lake) in Ladakh, NW Himalaya: a response of late Holocene aridity

Pradeep Srivastava<sup>1,\*</sup>, Anil Kumar<sup>1</sup>, Randheer Singh<sup>2</sup>, Oshin Deepak<sup>3</sup>, Arjit M. Kumar<sup>3</sup>, Yogesh Ray<sup>4</sup>, R. Jayangondaperumal<sup>1</sup>, Binita Phartiyal<sup>2</sup>, Poonam Chahal<sup>1,5</sup>, Pankaj Sharma<sup>1</sup>, Rupa Ghosh<sup>1</sup>, Naresh Kumar<sup>5</sup> and Rajesh Agnihotri<sup>2</sup>

<sup>1</sup>Wadia Institute of Himalayan Geology, Dehradun 248 001, India

<sup>2</sup>Birbal Sahni Institute of Palaeosciences, Lucknow 226 007, India

<sup>3</sup>Department of Geology, Lucknow University, Lucknow 226 007, India

<sup>4</sup>National Centre for Polar and Ocean Research, Goa 403 802, India

<sup>5</sup>Department of Geology, HNB Garhwal University, Srinagar 249 161, India

**Pangong Tso is a brackish water lake that lies along Pangong strand of the Karakoram strike-slip fault in arid Trans Himalayan region. The geomorphic mapping along the periphery of the lake suggested the presence of four palaeolake level strands located at 6, 4.8, 3.8 and 1.25 m above the present lake level. The gullied periphery expose relict deltaic sediments where sedimentological study enabled us to identify four deltaic lobes that make a classic Gilbert-type delta with well-developed top-set, fore-set and bottom-set. The top-set of the stratigraphically oldest delta lobe that corresponds to the highest lake level shows the presence of freshwater molluscs identified as *Radix* and a burnt sediment layer (hearth). The charcoal derived from this layer yielded <sup>14</sup>C date as 1.7 ka BP and six luminescence ages from different delta lobes suggested that delta evolution and lake level fall of ~6 m took place between ~2–1 ka. Review of palaeoclimate record available from NW Himalaya and Pangong Tso suggests that late Holocene aridity might be responsible for this rapid lake level fall. Sclerochronological analysis carried out on 54 subsamples from three *Radix* specimens suggested that the modern type of seasonal conditions may have prevailed at ~1.7 ka BP.**

**Keywords:** Ladakh Himalaya, Lake-Delta, Late Holocene aridity, Pangong Tso, Sclerochronological analysis.

## Introduction

HIGH altitude lakes are sensitive to climate change and prone to marginal shifts in the precipitation–evaporation (P–E) balance of its catchment areas<sup>1</sup>, therefore the strand lines and delta sequences of lakes can provide evidence of past climate variability. Literature indicates that the

lake basin experiences effects not only due to climatic variation (local and global; changes in precipitation–evaporation balance over the catchment area), but also, at times, due to non-climatic factors such as tectonic activity, changes in local catchment morphology and anthropogenic activities, which are also important determinants<sup>2–5</sup>. The Tibetan Plateau (TP) hosts more than 833 lakes distributed all over the plateau with a size of >1 sq. km (ref. 6). Pangong Tso (Tso is the term used for a lake regionally), ~145 km long, trans-boundary, brackish lake is shared between India and China. It is located on the SW-edge of the Tibet at an altitude of 4250 m amsl (above mean sea level) in arid Trans Himalaya where tectonics can also play a dominant role in varying the lake levels. The lake follows an active strand of strike-slip Karakoram Fault. The study of such a lake that lies in the climate sensitive and tectonically active region is a potential candidate to evaluate climate–tectonic causes impacting lake levels. Geomorphic mapping of strand lines coupled with sedimentology and chronology of Pangong Tso delta, thus can be decisive on climate or tectonic controlled factors of the lake levels. This study maps the strand lines using Differential Global Positioning System (DGPS) and provides a sedimentological account of the exposed lake delta. The chronological constraints are provided using Optically Stimulated Luminescence (OSL) and convention radiometric <sup>14</sup>C dating techniques. We also provide a review of Holocene climate variation and evaluate the past lake levels in light of palaeoclimatic variation in the region.

## Climate and geology of the study area

The lake is situated in eastern Ladakh with a catchment area of about 2000 sq. km with its aerial extent being around 650 sq. km with the maximum width of the lake being ~8 km on the Indian side, but an average width of

\*For correspondence. (e-mail: pradeep@wihg.res.in)

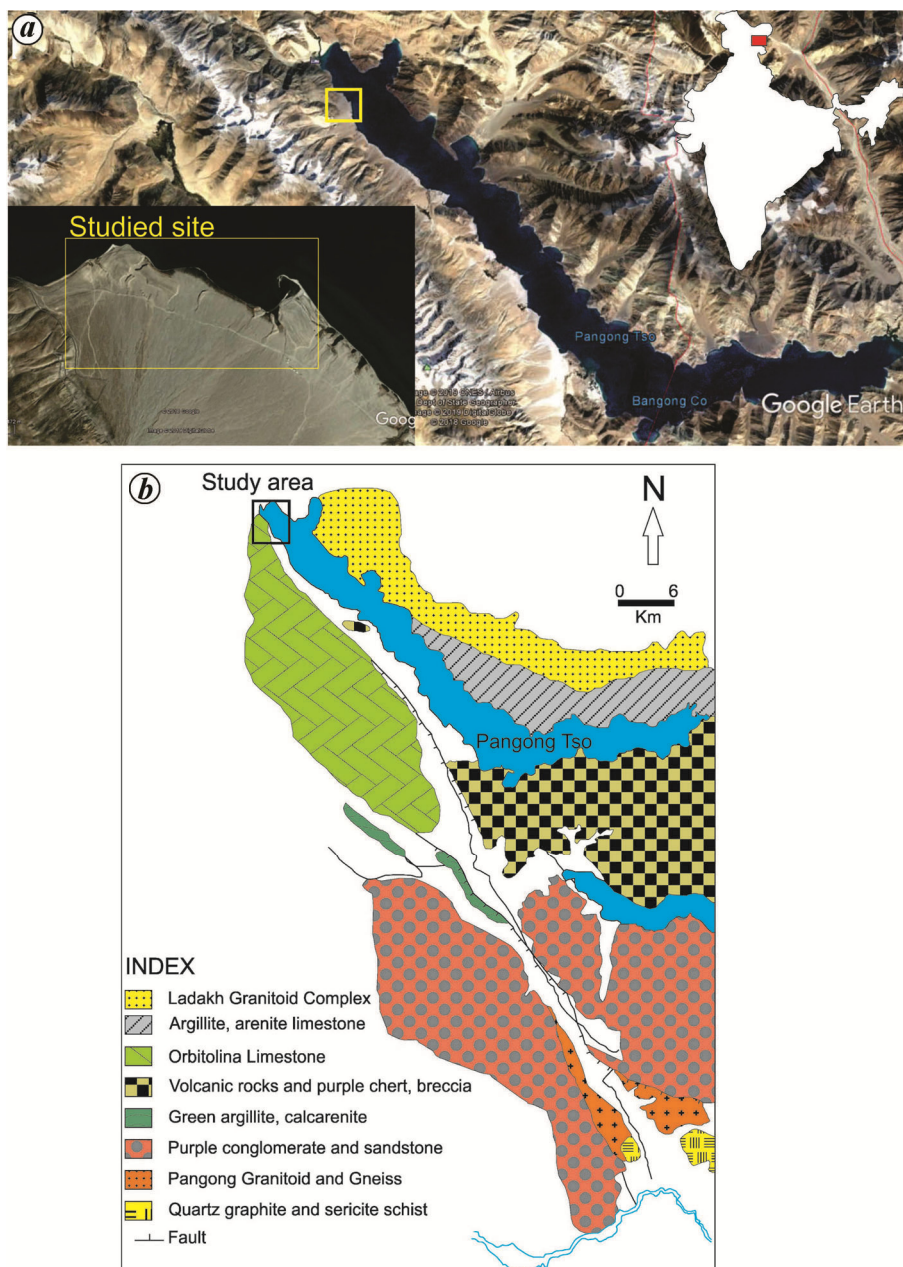


**Figure 1.** (a) Geomorphology and location and (b) geology of Pangong Tso area.

~3 km. It is part of a series of 5 lakes, called the Tso-mo-gualari. The lakes are separated by alluvial fans or deltaic deposits, and the whole series may be regarded as a single, closed basin. The study area lies at the western extremity of the lake ~100 km east of Leh (Figure 1). The lake receives water from snow-fed streams and has moderate alkaline water of pH >9 (refs 7, 8). Depending on the length of the melting season, fresh water input alternating between saline/brackish and fresh water, modulates the lake level and its pH conditions<sup>9,10</sup>. The lake catchment receives an average ~75 mm annual precipitation, whereas the ambient temperature of the area varies between -40°C and ~20°C as minimum and maximum temperature respectively.

The entire region of Ladakh is in the rain shadow of the NW Himalaya and has an arid to hyper-arid climate and dry steppe vegetation<sup>11,12</sup>. The study area is a high altitude cold desert that experiences severe winter and is covered with snow for three to four months from November to February. Winter westerly winds, associated with the subtropical branch of the Northern Hemisphere westerly jet<sup>13</sup> bring moisture from the Mediterranean region, which is the dominant source of precipitation in the form of snow. The moisture transported by the Indian Summer Monsoon (ISM) winds occasionally reaches the region. The spatial coverage and intensity for both the wind systems are dominantly influenced by the position of Inter-tropical Convergence Zone (ITCZ)<sup>12,14</sup>. The mean annual

precipitation of 100–300 mm is recorded at Leh weather station<sup>15</sup>. Studies reveal that the contribution by the westerly-associated air masses to the regional moisture budget has a remarkably decreasing trend towards the east and southeast in Ladakh<sup>16,17</sup>.

The lake basin comprises a variety of geomorphological features such as past deltaic deposits, beaches, alluvial fans (Figure 1a) deposited by meltwater as well as stranded shorelines and terraces. These deltaic deposits, terraces and palaeo-strandlines are evidence of the highest lake-level in the past. The southern bank of the lake surface is covered by ~5 m thick mud and finely laminated sand<sup>18</sup>, and the moraine deposits at the western end<sup>19</sup>.

Geologically Pangong Tso is located in a pull-apart basin between two strands of a large scale dextral strike-slip fault, i.e. the Karakoram Fault. The two strands are the Pangong strand and the Tangtse strand. The northwestern basin of Pangong Tso is structurally controlled by oblique slip faulting along the Pangong strand of the Karakoram Fault. The southwestern branch, the Tangtse strand, runs through Darbuk and Tangtse villages towards Chusul and is the major fault which separates the Karakoram rocks to the northeast from pre-collisional Ladakh granites (Figure 1b). Between the two strands, a variety of migmatites and high-grade metamorphic rocks including amphibolites, orthogneisses, calc-silicates and rare pelites are exposed. The Pangong Range bounded by the active Pangong strand and the catchment area of Pangong Tso mainly consists of rocks of Pangong Group, Karakoram Metamorphic Complex, is comprised of mainly slate, mica schist, greenschist/amphibolites and marble, calc-silicate and a band of mylonitised granite gneiss<sup>20,21</sup>. A belt of low-grade metamorphics having many marble bands with the presence of a dominant suite of greenschist/amphibolite and calc-silicates are extensively developed on the banks of lake<sup>20,21</sup>.

## Methodology

Pangong Tso lake margins are gullied and expose good vertical and lateral litho-sections of lake-delta sediments. Geomorphologically the southern bank is identifiable into several palaeolake strand lines. Lake-delta was studied for its sedimentology and chronology. Further, gastropod shells collected from the delta sequence were subjected to isotopic and sclerochronological analysis. The study area was mapped using total station theodolite (TST) to identify various strandlines with accurate elevation. The details of the methodologies are given below.

### *Sedimentology*

Sedimentary parameters such as grain-size, colour, physical structures, degree of bioturbation and lateral geometry of depositional units were utilized to decipher the sedi-

mentary environment of the delta. Grain size analysis of bulk samples was done using Laser Diffraction Particle Analyser (Malvern Mastersizer 2000MU). Prior to the analysis, all samples were subjected pre-chemical treatment by 10% HCl, followed by 40% H<sub>2</sub>O<sub>2</sub> to remove carbonates and organic material respectively. During the measurement, samples were disaggregated in distilled water, with 2300 rpm stirrer and 40% ultrasonic vibrator for 45 seconds.

### *Mapping of lake strand lines*

A Leica Viva TS12 Robotic TST with a precision of few millimetres was used with a GRZ4, 360° reflector fitted on a surveying pole to map the fine details of the lake strand lines at an ideal location (where the original topography was not modified due to natural processes or anthropogenic reasons) in the NW of Pangong Tso. In order to register the fine topographic perturbation particularly the strandlines (marks of the palaeowater-level) of the lake, we made regular observations to obtain an array of closely spaced points. These points have information of X, Y and Z coordinates in metres, and those were imported in GIS to create the contour lines by interpolation (kriging). To simplify the output topography, we removed the noise and artifact manually and assigned the altitude values considering the lake surface as a local datum, i.e. at 0 meter and contours were generated (Figure 2a). The cross-section (Figure 2b) is the plot of the Z versus X coordinates, which in this case are the distance and altitude (m) from the water surface respectively, that helped in identifying the strandlines.

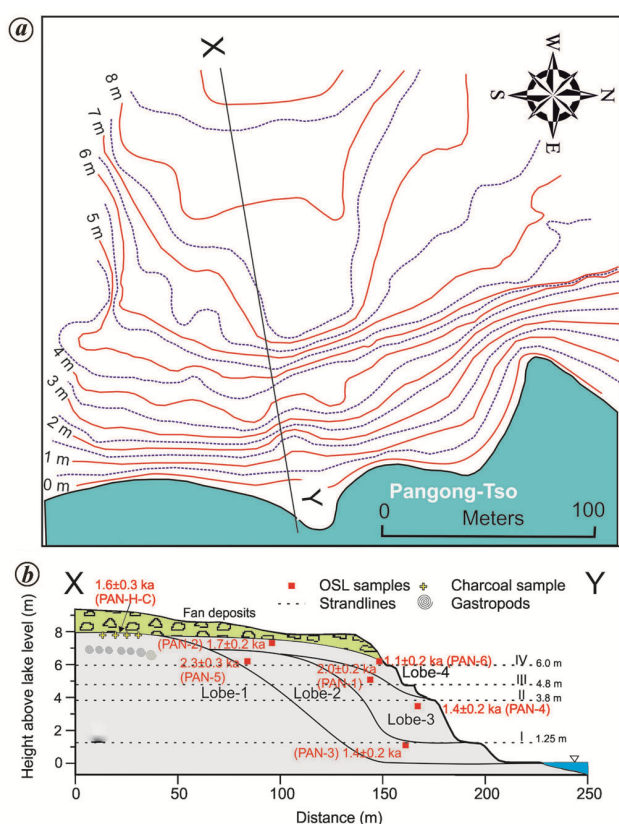
### *OSL sample collection and dating*

Delta sequence exposed in the western side of the present day lake was selected for the OSL sample collection. A total of six samples (PAN-1 to PAN-6) were collected from different lobes of a palaeodeltaic deposit. The details of the sections and stratigraphic positions of the samples are given in Table 1.

Quartz fraction of samples was extracted by treating them sequentially with 10% HCl, 30% H<sub>2</sub>O<sub>2</sub> followed by heavy liquid separation using sodium polytungstate (density = 2.67 g/cm<sup>3</sup>) and separation of quartz from feldspar using sodium polytungstate of density 2.62 g/cm<sup>3</sup> (refs 22, 23). These grains were then sieved to extract the 90–150 μm fractions. The sieved fraction was etched using 40% HF for 80 min followed by 20 min treatment with 35% HCl to remove alpha irradiated outer skin and residual feldspars. The purity of quartz vis-à-vis feldspar contamination was tested using infrared stimulated luminescence (IRSL). Quartz grains were mounted on stainless-steel discs using Silko-Spray silicone oil, and 40 aliquots were prepared for luminescence analysis. Low

**Table 1.** Radiocarbon and luminescence age data from the samples collected from Lake Delta sediments of Pangong Tso

Delta lobe	PAN-H	PAN-5	PAN-3	PAN-1	PAN-4	PAN-2	PAN-6
	Lobe-1	Lobe-2	Lobe-2	Lobe-3	Lobe-3	Lobe-4	Lobe-4
Lab no.		LD-3094	LD-3092	LD-3090	LD-3093	LD-3091	LD-3095
Depth (m)		3.0	9.0	1.7	5.6	1.0	2.4
U (ppm)		2.7	1.3	1.0	2.2	2.1	2.4
Th (ppm)	Uncalibrated C <sup>14</sup>	9.7	11.1	8.2	11.4	8.1	9.5
K (%)	charcoal age	2.1	2.2	2.1	2.2	2.2	2.6
Moisture (%)	1.7 ± 0.2 ka;	5 ± 3	5 ± 3	5 ± 3	5 ± 3	5 ± 3	
Mean ED (Gy)	1.6 ± 0.3 calibrated age	8.1 ± 1	4.4 ± 0.5	5.6 ± 0.5	4.8 ± 0.5	5.7 ± 0.5	4 ± 0.6
Weight mean ED (Gy)		7.7 ± 1	4.3 ± 0.5	5.6 ± 0.6	4.8 ± 0.4	5.6 ± 0.5	4 ± 0.6
Number of aliquots		27	31	32	25	27	28
Overdispersion (%)		0.0	10.0 ± 0.3	8.2 ± 0.2	8.4 ± 0.3	9.0 ± 0.3	14.9 ± 0.4
Dose rate (mGy/ka)		3.3 ± 0.1	3.1 ± 0.1	2.8 ± 0.1	3.3 ± 0.1	3.2 ± 0.1	3.7 ± 0.1
Mean age (ka)		2.5 ± 0.3	1.4 ± 0.2	2 ± 0.2	1.4 ± 0.2	1.8 ± 0.2	1.1 ± 0.2
Weight mean age (ka)		2.3 ± 0.3	1.4 ± 0.2	2 ± 0.2	1.4 ± 0.2	1.7 ± 0.2	1.1 ± 0.2

**Figure 2.** (a) Contour map of the lake periphery and (b) cross section along X–Y showing four lake strands of Pangong Tso and chronology.

luminescence sensitivity in some samples necessitated the use of large aliquots. Luminescence measurements were made in a Riso TL/OSL-DA-20 mini-system with an array of blue LEDs stimulation.

The signal was recorded through an optical filter U-340 for 40 sec at 125°C elevated temperature. Palaeodose was estimated using a 5-point single aliquot regeneration protocol of Murray and Wintle<sup>24</sup>. A preheat of 220°C for 10 sec was selected using preheat plateau and dose recovery tests. The weighted mean palaeodose was calculated incorporating recycling ratio 10% and recuperation ratio <5%.

The quartz examined shows a typical shine down curve with an exponential growth curve<sup>25</sup>. Initial 7 channels were used for age calculation, whereas the last 50 channels were considered as background. The uranium (<sup>238</sup>U), thorium (<sup>232</sup>Th) and potassium (K) concentrations were measured by X-ray fluorescence. The cosmic gamma contribution was calculated following Prescott and Stephan<sup>26</sup>, and water concentration was assumed to be 5 ± 3% by weight.

#### <sup>14</sup>C Dating

A charcoal sample (PAN-H) collected from the top-set of the oldest delta lobe, was dated using <sup>14</sup>C dating technique using a traditional beta counting of prepared liquid benzene (C<sub>6</sub>H<sub>6</sub>) at the Birbal Sahn Institute of Palaeosciences (BSIP), Lucknow, India. The sample was treated with 1% HCl at 80°C for 1 h on a water bath and then washed with deionized water to remove inorganic carbonates. Dried powdered sample was used to prepare C<sub>6</sub>H<sub>6</sub> using established laboratory protocols<sup>27</sup>. Prepared liquid C<sub>6</sub>H<sub>6</sub> was kept in deep freezer for about a week before counting, allowing decay of short lived radio isotopes. Then a liquid scintillation counter (QUANTULUS 1220) was used for counting the decay of <sup>14</sup>C present in the analyte. Radiocarbon ages of samples (BSIP laboratory number BS-4071) were estimated to be 1710 ± 200 years BP (Table 1). The age was calibrated using Intcal13.14c software<sup>28</sup> to obtain calibrated calendar ages.

#### Sclerochronological analysis

The molluscan shells that have been used for the sclerochronological analysis are gastropod shells. The shells collected from the top-set of the Lobe-1 have been identified as pulmonate aquatic gastropods of the genus *Radix* Montfort, 1810 and belonging to the Lymnaeidae family-Rafinesque<sup>29</sup>. Three aragonitic/calcitic shells of *Radix* of varying sizes were taken and numbered as A, B

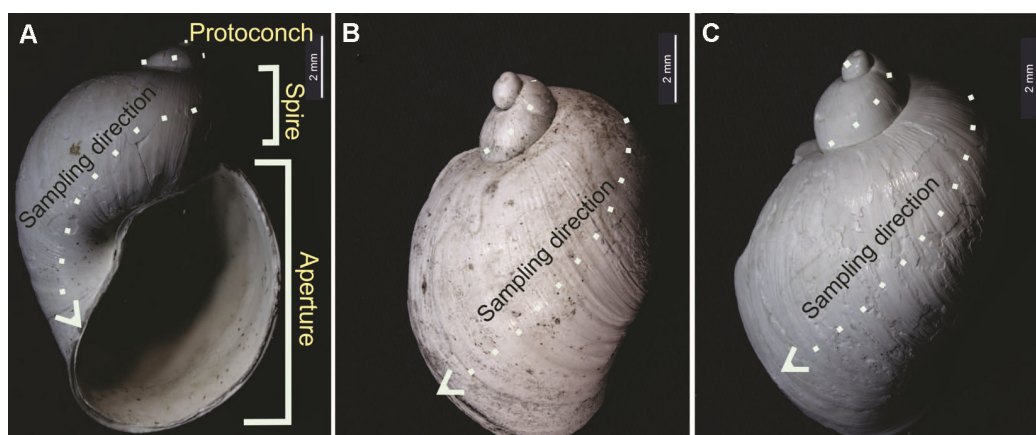


**Figure 3.** Three mollusc specimens shells A–C of *Radix* sp. collected from highest lake stand and delta top-set. The white arrow shows the direction of sub sample collection.

and C (Figure 3). These shells were photographed under a stereo zoom binocular microscope (LEICA) and weighed up to 4 decimal places. The shells were then cleaned of all impurities such as silt and clay particles by an ultrasonic bath for 3–5 min. After that, they were immersed in 30% H<sub>2</sub>O<sub>2</sub> (hydrogen peroxide) for 24 h to remove all organic matter such as the periostracum. The specimen was then washed, dried at room temperature for 24 h, weighed and photographed. Clean shells were sub-sampled at close intervals by scratching along each growth line, progressively from the protoconch to the aperture, i.e. from the oldest to the youngest part. The interval between each sampling was ~1 mm, and about 15–20 samples were taken from each shell.

About 100–200 µg of the sample were taken into the clean Labco Examiner vials (12 ml). Every vial was flushed through helium (99.99% He) to remove the atmospheric gases present in the head space. The  $\delta^{13}\text{C}$  and  $\delta^{18}\text{O}$  measurements were carried out by standard equilibration method in which biogenic shell was equilibrated with CO<sub>2</sub> with known isotopic composition. The sample was kept in a thermostatic sampling tray maintained at temperature 72°C on a gas-bench system to achieve complete equilibration for one hour. The equilibrated CO<sub>2</sub> was then introduced into the Thermo Fisher Delta V plus isotope ratio mass spectrometer for measuring the isotope ratios. The stable isotope ( $\delta^{13}\text{C}$  and  $\delta^{18}\text{O}$ ) measurement of the reference gas CO<sub>2</sub> (99.99%) were calibrated against International Standard IAEA-NBS-18 VPDB. The accuracy and reproducibility of measurements were checked with in-house standard CaCO<sub>3</sub> (Merck) and repeat measurements which were better than 0.1‰ for both  $\delta^{13}\text{C}$  and  $\delta^{18}\text{O}$ .

## Results

### Geomorphology

Pangong Tso is a chain of five basins separated by shallow sills and evolves as a series of lakes with connecting

ridges<sup>30</sup>. Sub-basins are ~40 m deep and connecting sills are at a depth of 1–2 m below the present lake surface<sup>31</sup>. It runs between two mountain ranges in the NW to SE direction which steadily widens towards the south of south-east, before bending eastward into China (Bangong Co). Presently, the lake is a closed basin lake<sup>32</sup> and series of ancient shoreline ring the basin. In the historical accounts of the early expedition of the pre-industrial era, some ancient shorelines are recognized lying 260 m above the present-day level<sup>33</sup>.

These distinct stranded shorelines and terraces along the basin indicate former high stands of this lake and provide information about the wider extent of the lake area in the past<sup>34</sup>. Two well-preserved shorelines on the NE side of Pangong Tso at ~4266 (+19 m above present level) and ~4300 m amsl can be seen clearly in high resolution Google Earth imagery that are also recognizable on the northern bank of the lake<sup>20</sup>. The present lake level, in the studied western sector, lies at 4247 m amsl. In the eastern sector of the lake, a 79 m high lake terrace lying at 4320 m amsl is dated to 30–40 ka (refs 35, 36).

Total station theodolite mapping indicates the presence of four distinct stranded shorelines present along the southern margin indicating palaeo-high stands numbered as I–IV and measured at an elevation 1.25, 3.8, 4.8 and 6.0 m from the present day lake level (4247 m amsl; Figure 2b). Further, a large number of glacial melt-water feeder channels, from both north and south, supply sediment and water to the Pangong Tso. The glaciers at southern ridge are closer to the lake margin. Therefore, approximately 30 large fans prograde toward the lake and contribute large amount of sediment from this side.

### Chronology

The equivalent doses, dosimetry, dose rates and luminescence ages of all samples are presented in Table 1 and OSL characteristics are shown in Figure 4. The OSL age determination and samples analysed from different levels

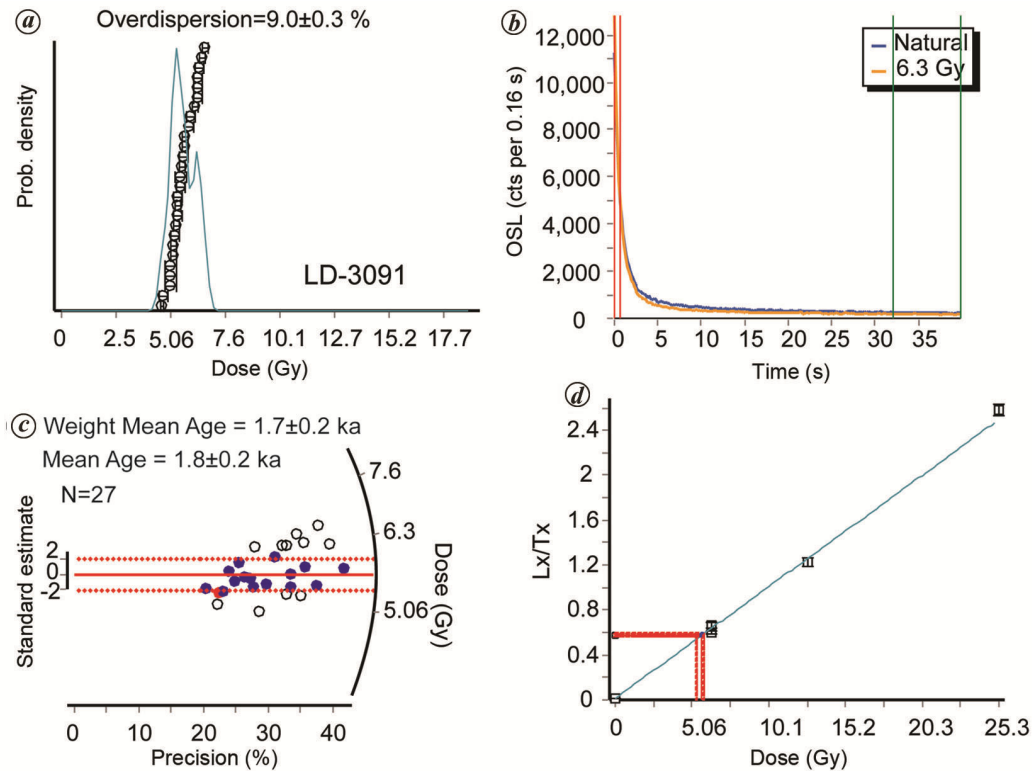


**Figure 4.** (a) Probability distribution, (b) Shine down, (c) Radial plot and (d) Growth curve for OSL sample LD-3091.

are shown in Figure 2 *b*. The charcoal collected from the hearth present in the top-set of Lobe-1 yielded a  $^{14}\text{C}$  age of  $1.6 \pm 0.3$  ka. The Lobe-2 yielded OSL ages of  $2.3 \pm 0.3$  ka (PAN-5) and  $1.4 \pm 0.2$  ka (PAN-3). Likewise, the Lobe-3 yielded OSL ages of  $2 \pm 0.2$  ka (PAN-1) and  $1.4 \pm 0.2$  ka (PAN-4). Lobe-4, stratigraphically the youngest, yielded ages of  $1.6 \pm 0.3$  (PAN-2) and  $1.1 \pm 0.2$  (PAN-6). The chronological data shows that all the ages are overlapping and implying rapid progradation of delta and lobe formation, and it is beyond the limits of dating technique to resolve. Nonetheless, the  $^{14}\text{C}$  age of  $1.6 \pm 0.3$  ka from Lobe-1 and  $1.1 \pm 0.2$  ka (PAN-6) of Lobe-4 can be taken as lower and upper bound chronology implying the delta progradation and lake level fell between  $\sim 2$ –1 ka.

#### Lake delta sequence

High-resolution mapping of the lake periphery suggested the presence of four lake strands with highest being located at  $\sim 6$  m above the present day lake-level. Several streams carrying meltwater join the lake and build a fan that grades basin ward into a lake delta. The lake level lowering in recent past has resulted into the formation of four mapable strands and the incision by inlet streams provides good exposure of past deltaic sequence. The stratigraphy of the exposed delta exhibits four prograding delta lobes (Figure 5 *a*), where individual lobes are identifiable into a typical bottom-set, fore-set and the top-set

deposition. The sequence extends to about 250 m lake-wards.

The top-set is made up of horizontally bedded gravelly beds and sandy scoured channels. The gravel beds internally are parallelly laminated and composed of platy, rounded to sub-rounded, moderately sorted lithic fragments of 1–5 cm diameter (Figure 5 *b*). The sandy channels are up to 3 m wide and 1.5 m thick, fining upwards with poorly sorted gravels at the base whose top  $\sim 50$  cm is bioturbated clayey silt showing convolute bedding. The horizontally bedded gravelly unit may represent sub-areal deposition in the beach environment of the lake whereas the channelized units form part of fan made by feeder channel<sup>37,38</sup> that get bioturbated during the low stages. Bioturbated clayey silt units may suggest the presence of small pond/lagoon where convolute beddings may form due to cryoturbation as a result of seasonal freezing and thawing.

The delta fore-set is composed of 1–2 cm thick beds that dip in basin ward direction to  $5^\circ$ – $10^\circ$  (Figure 5 *a*). At times fore-sets are lined with poorly sorted granule sized lithic fragments and development of wavy ripples. The beds internally are made up of couplets of poorly sorted, very fine sand unimodal coarse silt and exhibit high to moderate degree of plant and animal burrow bioturbation. The plant burrows are fibrous and the animal burrows are tubular with swollen nodes. At places, these burrows are 5–10 cm thick faintly laminated or massive silty beds that may show lateral discordances.

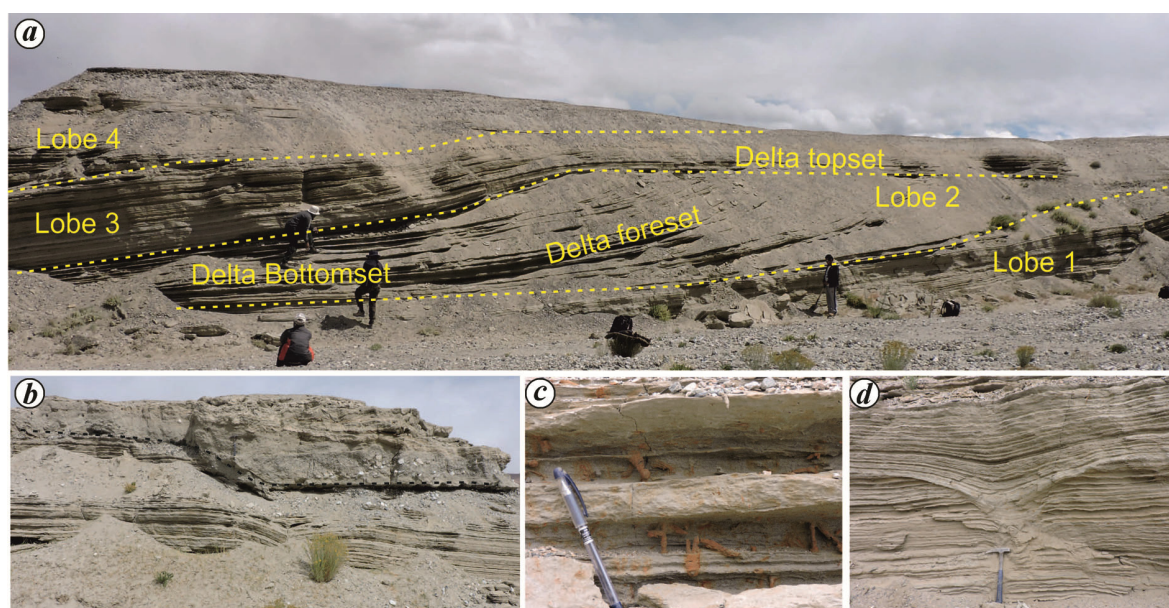


**Figure 5.** *a*, Transverse section of Deltaic deposit exposed at the Pangong Tso bank showing four delta lobes and well-developed top-set, fore-set and bottom set; *b*, Scoured channels in the top-set; *c*, Bioturbation in fore-sets; *d*, Scour and fill in the bottom-set.

The delta fore-sets are formed during delta front progradation under declining lake levels. The rippled sandy layers indicate sedimentation by traction bottom currents whereas silty layer is deposited as settling suspended load. The poorly sorted grain-size and presence of granule size grains in some layers indicate sedimentation due to turbidity currents as a result of increased sediment supply during summers whereas thick massive beds may indicate the sedimentation during storm conditions on the delta slope<sup>37,38</sup>. The dense bioturbation indicates phases of the low rate of sediment supply and sedimentation under sub-aqueous conditions.

The ~1 m thick delta bottom-set is composed of finely laminated, horizontal to sub horizontal clayey silt whose proximal part is tangential to the fore-set unit. The individual laminae are 1–5 cm thick and exhibit mottling. The mottle burrows in general, are vertical and range up to 10 cm in length and 1 cm diameter (Figure 5 *c*). The bottom-set units are often seen truncated by scour and fill structure that range up to a metre in size (Figure 5 *d*).

The exposed delta complex is identifiable into four, progressively smaller in size, prograding delta lobes that explicitly exhibit the top-set, fore-set and the bottom-set of Gilbert type delta structure. Figure 5 *a* exhibits an E–W trending exposed section of delta complex showing lateral and vertical juxtaposition of four lobes. The mean grain size decreases overall from Lobe 1 to Lobe 3 and slightly increases in Lobe 4.

Lobe-1, the oldest one reaches up to an elevation of 6 m whose top-set shows preserved mollusc shell bed and occurrence of a hearth containing centimetre thick charcoal specks and rock fragments implying anthropogenic activity. The shells are identified as fresh water mollusc

*Radix* sp. (Figure 3). An earlier study<sup>10</sup> has also reported the occurrence of empty *Radix brevicauda*, *Radix lagotis* from the shorelines of Pangong Tso. The 0.70 m thick bottom-set is finely laminated and dips lake-ward at an average angle of 10°. Based on the degree of bioturbation ~2.5 m thick delta fore-set is internally divisible into several depositional phases. The bottom ~1 m, having 3–5 cm thick beds, exhibits typically horizontal burrows that are restricted to individual beds suggesting a high rate of sedimentation, restricted sub-aerial exposure giving lesser time for vertical burrowing. The upper ~1.5 m is relatively densely bioturbated with burrows penetrating 5–10 cm deep into more than four layers implying a low rate of sedimentation. Lobe 2, ~2 m thick, is finer in grain size composition and exhibits lower degree of bioturbation as compared to Lobe 1. The top-set of this lobe is ~50 cm thick which shows presence of a discontinuous bed of well sorted gritty sand and parallel laminated clayey silt. The fore-set of Lobe-2, in turn is 1.5 m thick and dips lake-ward direction at an average angle of 30° (Figure 5 *a*). A ~50 cm thick bottom-set finely laminated, is made up of couplets of thick sandy (~5 cm) and finer silt layers. Lobe 3, sits with a discordance of ~30° indicating avulsion of feeder channel. The top-set of this lobe is relatively sandy and highly oxidized and shows a high degree of bioturbation. The fore-sets are showing frequent thick beds of rippled fine sand (3–8 cm) that is capped by thin silty layer (~2 cm) and exhibit a high degree of bioturbation with burrows penetrating deep into several beds. The fore-set laminae merge laterally into the fine grained, 30 cm thick, bottom-set. This indicates delta progradation of this lobe occurred with frequent sub-aerial exposures and more arid conditions.

**Table 2.** Stable isotope data of subsamples collected from three shells

Shell A			Shell B			Shell C		
Sample	$\delta^{13}\text{C}$ ‰	$\delta^{18}\text{O}$ ‰	Sample	$\delta^{13}\text{C}$ ‰	$\delta^{18}\text{O}$ ‰	Sample	$\delta^{13}\text{C}$ ‰	$\delta^{18}\text{O}$ ‰
A1 (ptc)	-0.29	2.61	B1 (ptc.)	-0.59	-0.06	C-1(ptc.)	0.29	2.31
A2	0.91	3.32	B2	-0.77	0.01	C-2	-0.34	2.14
A3	-1.56	1.06	B3	-2.08	0.07	C-3	0.08	1.72
A4	-0.51	1.75	B4	-1.87	0.47	C-4	-0.31	1.21
A5	-0.57	0.41	B5	-1.67	0.82	C-5	-1.15	0.80
A6	-0.70	0.42	B6	-2.14	0.91	C-6	-0.96	1.04
A7	-0.32	1.85	B7	-1.57	1.18	C-7	-0.66	1.15
A8	-0.26	1.80	B8	-1.49	1.50	C-8	0.33	2.13
A9	0.18	2.44	B9	-1.47	1.30	C-9	-1.49	1.41
A10	-0.62	1.83	B10	-1.04	1.77	C-10	-1.38	1.87
A11	0.01	2.65	B-11	-0.92	2.18	C-11	-1.43	1.50
A12	-0.06	0.47	B-12	-0.74	2.35	C-12	-0.71	1.35
A13	-0.69	1.43	B-13	-0.75	2.54	C-13	-0.15	1.47
A14	-1.07	0.13	B-14	-0.43	2.54	C-14 (ap.)	0.55	0.44
A15	-0.95	1.14	B-15	0.04	2.98			
A16	-1.35	0.12	B-16	0.06	1.98			
A17	-2.25	-1.84	B-17	-1.32	1.37			
A18	-0.88	1.45	B-18	-1.47	0.83			
A19 (ap.)	-1.25	1.20	B-19	-1.78	0.80			
			B-20	-1.93	0.75			
			B-21 (ap.)	-0.82	1.12			

Lobe 4 is ~2 m thick with ~90 cm thick top-set, which is made up of moderately well sorted gravels and parallel laminated gritty sand, making thick beach deposit. This, at places, is seen scoured by ~70 cm thick, moderately bioturbated channelized rippled fine sand units. The unit grades downwards into parallel laminated silt and gradually merges to lake-ward dipping delta fore-set. The fore-sets of its lobes are composed of sand-silt couplets where sandy layers are rippled and range up to 13 cm in thickness and silty layer up to 3–4 cm. The bottom-set is ~26 cm thick made up of finely laminated, highly bioturbated coarse silt. The entire sequence is overlain by fan sediment deposited by feeder channel.

The older fan deposits consist of very coarse grit and alternate with 6–7 cm thick gravel beds. The younger fan deposit consists of grey sand with alternating ripples and parallel laminated at the top.

### *Sclerochronological analysis*

The highest lake strand corresponding to delta Lobe 1 contains freshwater molluscs that are identified as *Radix*. These molluscs are known to occur widely in high altitude regions of Himalaya and Tibet and the earliest fossil records of this family are known since the middle Jurassic<sup>39</sup>. The *Radix* is a widely distributed invertebrate and is adapted to extreme conditions like high altitude, extended ice cover periods on the water bodies or extreme temperature variations<sup>40,41</sup>. The life span is assumed to be 1–2 years, but a longer life span cannot be excluded because under cold-water conditions embryogenesis and ontogeny in general can be extremely prolonged<sup>40</sup>. Shell accretion occurs during all seasons; size increase is much lower

during the winter but does not cease<sup>42</sup> and hence its stable carbon and oxygen isotopic inventory and ratios archive weather (seasonal) pattern that may have existed during their life span.

Three well developed shells named as shell A, B and C were subsampled for isotopic analysis and described below ontogenetically from the embryonic shell (protoconch) which is formed prior to hatching, to the latest part of the shell (aperture) and shown in Figure 3. The growth direction of the shell is from protoconch to aperture. Table 2 provides data on stable isotopes of carbon and oxygen from the subsamples collected from three *Radix* specimens, viz. shell A, B and C the details are described below:

*Shell A:* Nineteen subsamples were collected from this shell, where A1 is the protoconch and A19 is the aperture. The average  $\delta^{18}\text{O}$  value for the protoconch (A1) is 2.61‰. The value increases to 3.32‰ for the juvenile. A subsequent decreasing trend in values is observed up to sample A6 (0.42‰). This is followed by a multi-step increase up to sample A11, with a value of 2.65‰. This is followed by a sharp decrease from A11 to A12, from 2.65‰ to 0.47‰. The values remain low with minor fluctuations up to A16, which is followed by a further decline to A17. This is the point of the most depleted  $\delta^{18}\text{O}$  signal, with a value of -1.84‰. The terminal part of the shell, i.e. A18–A19 shows a sharp increase in the values of  $\delta^{18}\text{O}$ , up to 1.20‰ in A19 (Figure 6a).

The  $\delta^{13}\text{C}$  values of the protoconch are -0.29‰. There is an increase in the values in the early juvenile stage, from A1 to A2, followed by a sharp decrease from A2 to A3, where it becomes -1.56‰. The values then increase

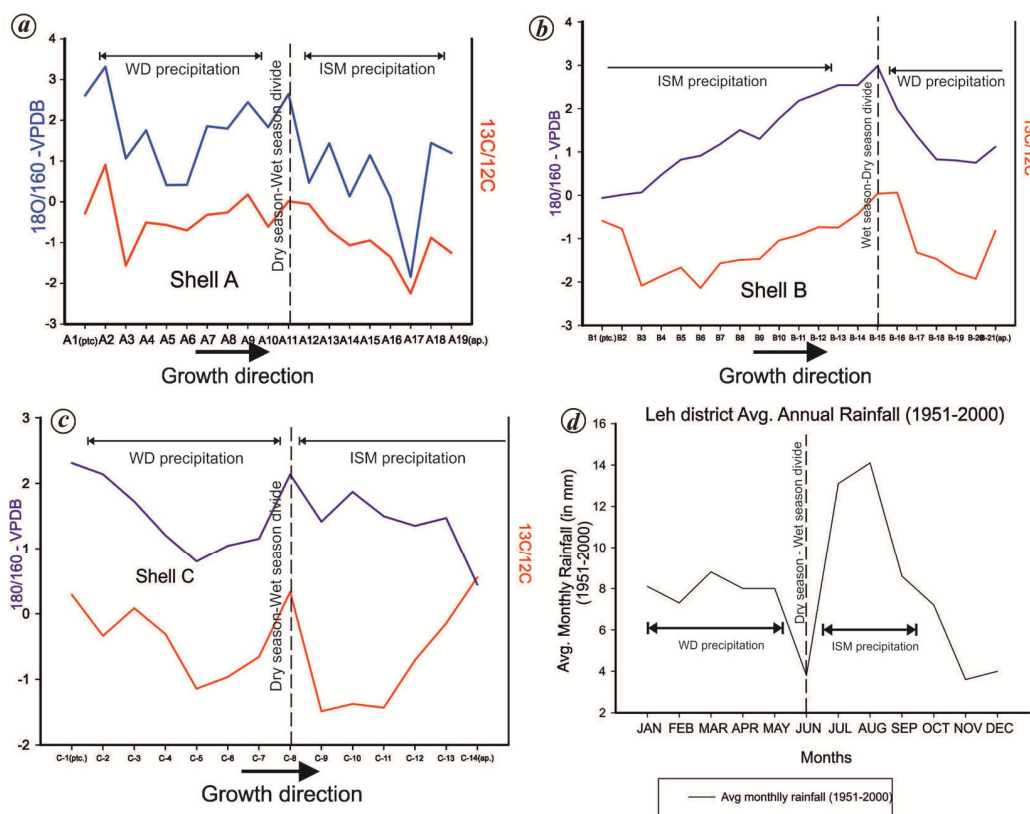


**Figure 6.** Stable isotope data (a) Shell A, (b) Shell B, (c) Shell C and (d) rainfall distribution across the year (source: IMD).

gradually through the middle juvenile stage (A3 to A12), followed by a gradual decline in the middle stage and the values decrease up to A17, where it is the least, at  $-2.25\text{‰}$ . The values then show an increase in the oldest stage to  $-1.25\text{‰}$  in A19 (Figure 6 a).

**Shell B (B1 to B21):** Twenty one subsamples were collected from shell B. The  $\delta^{18}\text{O}$  value of the protoconch (B1) is  $-0.06\text{‰}$ . There is a gradual and continuous increase in the values through the juvenile and middle stage, with the highest value at B15 ( $2.98\text{‰}$ ) representing the middle stage. This is followed by a sharp decline in the values through the late stages of shell growth, between B15 and B18, where the values are between  $2.98\text{‰}$  and  $0.80\text{‰}$  respectively. The value remains low in the older stage, with an increase in the aperture value, B21 which becomes  $1.12\text{‰}$  (Figure 6 b).

The  $\delta^{13}\text{C}$  value of the protoconch is  $-0.59\text{‰}$ , and there is a sharp decrease in the values in the juvenile stages up to B6 ( $-2.14\text{‰}$ ). This is followed by a gradual and continuous increase in the values through the middle stage, up to  $0.06\text{‰}$  in B16. Another sharp decline in the values occur at B17, and the values remain low for a period of growth in the old stage, till B20 ( $-1.93\text{‰}$ ). The value then increases sharply at the aperture to  $-0.82\text{‰}$  (Figure 6 b).

**Shell C:** This shell yielded only 14 subsamples (C1 to C14). The average  $\delta^{18}\text{O}$  value for the protoconch (C1) is

$2.31\text{‰}$ . This is followed by a multiphase decline in the values in the juvenile stage up to C5 where it becomes  $0.80\text{‰}$ . In the middle stages, a sharp increase between C7 and C8, from  $1.15\text{‰}$  to  $2.13\text{‰}$  is noticed. In the last stage of the shell growth, there is an overall decrease in the trend of values, with a decline at the last (aperture) stage, i.e. C14,  $0.44\text{‰}$  (Figure 6 c).

The  $\delta^{13}\text{C}$  value of the protoconch (C1) is  $0.29\text{‰}$ . The values in the juvenile stage show a gradual decrease (C2–C5), where C5 is  $-1.15\text{‰}$ . This is followed by an increase in the values in the middle stages of shell development, with values increasing up to  $0.33\text{‰}$  at C8. This is followed by a sharp decline in the older stages of shell development, with values dropping to  $-1.49\text{‰}$  at C9, and stays at low for a short period up to C11. This is followed by an increasing trend in the values in the older stages, with values increasing up to  $0.55\text{‰}$  at the aperture (Figure 6 c).

**Discussion**

Pangong Tso is one of the largest water bodies in the Trans Himalaya that responds to monsoon driven precipitation changes and tectonics of Karakoram Fault. The high resolution geomorphic mapping of the lake periphery indicated presence of four palaeolake level strands located at 6, 4.8, 3.8 and 1.25 m above the present lake level (4247 m amsl). The gullied lake margin exposes a

classic section of Gilbert type delta with a well-developed bottom-set, fore-set and top-set. The sedimentological mapping of the deltaic sediments indicated the presence of four prograding lobes of successively lower size. The topmost strand that corresponds to top-set of the oldest delta lobe exhibits the presence of a shell bearing bed consisting freshwater mollusc called *Radix* and burnt layer (hearth). This indicates that the lake, at the highest strand, which at present is saline, was a freshwater body and possibly its banks were utilized for camping and cooking purposes. The  $^{14}\text{C}$  age of the charcoal derived from this hearth is dated to  $1.6 \pm 0.3$  ka. Likewise, the four deltaic lobes yielded luminescence ages between  $\sim 2$ – $1$  ka, suggesting active deltaic progradation and rapid lake level fell during this period (Figure 2). Earlier studies also reported five lake strands with the highest being  $\sim 20$  m above the present lake<sup>43</sup> and remote sensing based evidence of lake level fell in the region was recorded<sup>44</sup>. However, we differ from earlier work that interprets the delta as lacustrine sediments and that the incision of the sediments is caused by uplift along the strike-slip Karakoram Fault<sup>45</sup>.

#### *Holocene climate record of Ladakh Himalaya and lake level of Pangong Tso*

A large part of Ladakh and Tibetan Plateau remains in the rain shadow zone of SW Indian monsoon although during the strengthened monsoon phases, the area receives precipitation as rains. Annual rainfall distribution over Leh, as reflected by 50 years of precipitation data of India Meteorological Department (IMD), suggests significant control of SW Indian monsoon (Figure 6d). In relatively drier phases, it receives snow precipitation via westerlies and therefore the hydrology of lakes and rivers in the region is sensitive to variation in the strength of monsoon and westerlies. We review the Holocene climate record of the western Himalaya and SW Tibet to evaluate the role of climate in lake-level fall in Pangong Tso. The review has been divided on the basis of tripartite classification of the Holocene Epoch (early-Holocene, mid-Holocene and late Holocene) proposed by Walker *et al.*<sup>46</sup> by a working group of integration of ice-core, marine and terrestrial records (INTIMATE) and Sub-commission on Quaternary Stratigraphy (SQS) of the International Commission on Stratigraphy.

*Early Holocene (11,700–8200 cal yrs BP):* Pollen record from a peat deposit in Lahaul Spiti (NW Himalaya) suggests warm and moist climate  $\sim 10.5$  ka BP that continues throughout the early Holocene<sup>47</sup>. A SW monsoon driven glacial advance is reported  $\sim 11.5$ – $8$  cal yrs BP from Tibetan Plateau during and Himalayan region<sup>48–51</sup>. Studies on aeolian sand ramps in Ladakh region, due to the strengthened monsoon, exhibit gullying and formation of intradunal lakes between  $\sim 12$  and  $7$  ka BP (ref. 52). Mega

floods at  $\sim 11$ – $10$  ka BP are also reported from slack water deposit studies of Indus river system<sup>53</sup> inferring enhanced hydrological phenomena in the western Himalaya. Pollen record from Tso Kar by Demske *et al.*<sup>54</sup>, reported spread of *Artemisia*, suggesting strong influence of monsoon in the region during  $\sim 10.9$ – $9.2$  ka BP. Enhanced precipitation during  $\sim 11.5$ – $4.5$  ka BP is also suggested by palynological and carbon isotope record of lake Tso Moriri study<sup>55,56</sup>. Rising of lake level of Tso Kar from  $\sim 11.8$  ka BP and that reached to its maxima  $\sim 8.5$ – $7$  ka BP is reported<sup>57</sup>.

The palaeohydrologic and geomorphic studies of Pangong Tso-Tangtse indicate the existence of a larger lake basin during early- to mid-Holocene and a breach of a  $\sim 20$  m high spillway inducing a catastrophic flood in Tangtse valley at  $\sim 11$  ka (refs 58, 59). This flood was a result of monsoon driven lake breach during high-stand. Thus during the early Holocene strengthened SW monsoon, like the other lakes in Tibet, the Pangong Tso achieved the highest level as well.

*Mid-Holocene (8200–4200 cal yrs BP):* Pollen record of Chandra Tal shows a cold event from  $\sim 8.8$  ka to  $6.7$  ka BP which is followed by gradual strengthening of ISM that continued throughout the mid-Holocene<sup>47</sup>. Glaciological studies suggest that the mid-Holocene witnessed increased monsoon precipitation albeit summer cooling and enhanced glaciation in the Himalayan and Tibetan Plateau regions<sup>48</sup>. Enriched  $\delta\text{D}$  values of Pangong Tso at  $\sim 8.5$ – $7.5$  ka BP implied arid phase and lowering of lake-level<sup>60</sup>. Weakened ISM is reported from Tso Moriri Lake between  $\sim 8.5$  and  $\sim 5.5$  ka BP inferred from the appearance of endogenetic carbonates, aragonite, decreasing siliclastic Ti influx and isotopic enrichment of carbonates<sup>61</sup>. This is inferred as the results of declining solar insolation and southward displacement of ITCZ. Increased hydrological activity was found at  $\sim 4.5$  ka BP, while a cold-dry phase was witnessed at  $\sim 4.3$  ka BP that continues till the end of mid-Holocene as reported from another study of Tso Moriri<sup>62</sup>. Pollen and non-pollen palynomorph data of Tso Moriri indicates continued influx of freshwater till  $\sim 4.5$  ka BP followed by aridity and glaciation<sup>55</sup>. Demske *et al.*<sup>54</sup> suggest that this period is characterized by westerly influences and reduction of moisture supply inferred from the development of alpine meadow and desert steppe till  $\sim 4.8$  ka BP at Tso Kar. The lake experiences the highest water level around  $8$  ka BP as a result of both monsoonal and westerly influences. After  $\sim 4.8$  ka the lake experiences an abrupt shift to aridity. Lake Tso Kar shrank significantly after  $\sim 7$  ka BP and reached the lowest level at  $\sim 4.2$  ka (ref. 55). Majority of the study indicates fluctuation of climate in the mid-Holocene and arid/cold climate around  $4.2$  ka BP at western Himalaya. This was the time when  $\delta\text{D}$  values derived from leaf wax of Pangong Tso sediments (Bangong Co in China) gradually increased indicating weakening of SW monsoon<sup>60</sup>.

*Late-Holocene (4200 cal yrs BP to present):* Based on pollen records from lake, Lahaul-Spiti sequence suggests dry climate from ~4.3 to ~1.8 ka BP (ref. 63). However warm and wet climate prevailed between ~3.3 and 2 ka followed by cool and moist climate between ~2 and 1.1 ka as suggested by the peat record of Chandra Tal<sup>47</sup>. The record also archives a warm and wet phase of Medieval Climate Anomaly (MCA) and a cold phase corresponding to Little Ice Age<sup>47</sup> (LIA). Himalaya and Tibetan Plateau witness glacial advances at 550–530 years BP, 400–100 years BP and at 19th century<sup>48</sup> though the expansion of glaciers during LIA was lesser than that of the early-Holocene. Tree ring records from NW Himalaya and Karakoram also report long term droughts during the 15th and 17th centuries and a wetter phase during the end of 20th century<sup>64</sup>. At Tso Moriri, weakening of ISM continues from ~4.3 ka to 3.5 ka BP, where the period ~2.8–0.55 ka BP witnessed enhanced discharge as a result of intense ISM rainfall after which a cold-arid phase steps in, which coincides with LIA<sup>62</sup>. The weakening of ISM is also inferred from low pollen influx during ~2.8–1.3 ka BP at Tso Kar when lake-levels continued to drop<sup>54,57</sup>. However, droughts record from Tso Moriri suggests drought like conditions during ~4.6–3.9 ka BP and ~2.6–0.6 ka BP (ref. 61) and the palynological study also suggests the late-Holocene aridity continuing till ~1.8 ka BP (ref. 55).

Interestingly, our data on lake strands of Pangong Tso suggests the lake level fell ~6 m between ~2 and 1 ka, during when the salinity loving diatoms increased six fold in lake sediments (Figure 7a),  $\delta^{18}\text{O}$  of calcite showed a positive excursion of ~4‰ (Figure 7b), implying sharp decline in lake hydrology.  $\delta\text{D}$  values derived from leaf wax of lake sediments exhibited a significant positive excursion from -200‰ to -120‰ (Figure 7c)<sup>60</sup>. This suggests that the chronology of lake strands, delta sediments mirror the palaeolake environment.

*Sclerochronological analysis of molluscan shells*

The meteorological data of Leh from 1951 to 2000 (source: IMD) clearly shows that monsoon-driven precipitation starts picking up from June and achieves maxima around August and rainfall tapers to minimum in November (Figure 6d). The winter and early summer months receive westerly driven precipitation in the form of snow. The  $\delta^{18}\text{O}$  curves for the shells show two troughs, which reflect depleted  $\delta^{18}\text{O}$  values, and thus, possibly correspond to two phases of precipitation due to the dilution effect of the heavier O-isotope in the lake system during times of formation of the shell. Since there is no shut-down temperature of shell accretion in *Radix*, factors like time or season of accretion are neutralized. The trend of the  $\delta^{18}\text{O}$  and  $\delta^{13}\text{C}$  values in the direction of shell growth, i.e. from protoconch to aperture show a similar and parallel trend for all the three shells. Thus, it can be assumed that there was no change in the composition of the water

during shell formation. The IMD rainfall data from 1951 to 2000 was then compared with the isotope patterns, to determine the extent of change in temperature and precipitation regime which has occurred. The isotope curves are interpreted to provide an insight into the precipitation regime from ~2 ka and this has been compared with the contemporary data.

Two troughs can be observed in each curve of the  $\delta^{18}\text{O}$  values. Based on the width of the troughs in the  $\delta^{18}\text{O}$  values, the extent of ISM and westerly, over a period of approximately 1 year, can be inferred. The deeper trough (where  $\delta^{18}\text{O} < 0.00\text{‰}$ ) possibly represents the signals of ISM precipitation, enhanced melt-water input and the wet, summer season. These waters are more depleted due to the ‘amount effect’. Since Pangong Tso is a monomictic lake, i.e. the ice cover melts once a year, the higher  $\delta^{18}\text{O}$  values represent the melting season<sup>63,64</sup>. Generally, the  $\delta^{18}\text{O}$  values above 0.00‰ represent higher evaporation and reduced meltwater input and the dry, winter season. A trough in this part of the graph possibly signifies the period during which precipitation was brought in by the westerly during the winters, which has a less depleted signal. The dividing line drawn in all the graphs represents the driest period of the year post the westerly period, and can be inferred to as May, following which the ISM signal begins. The deeper trough post the dividing line in the curves represents the ISM precipitation period.

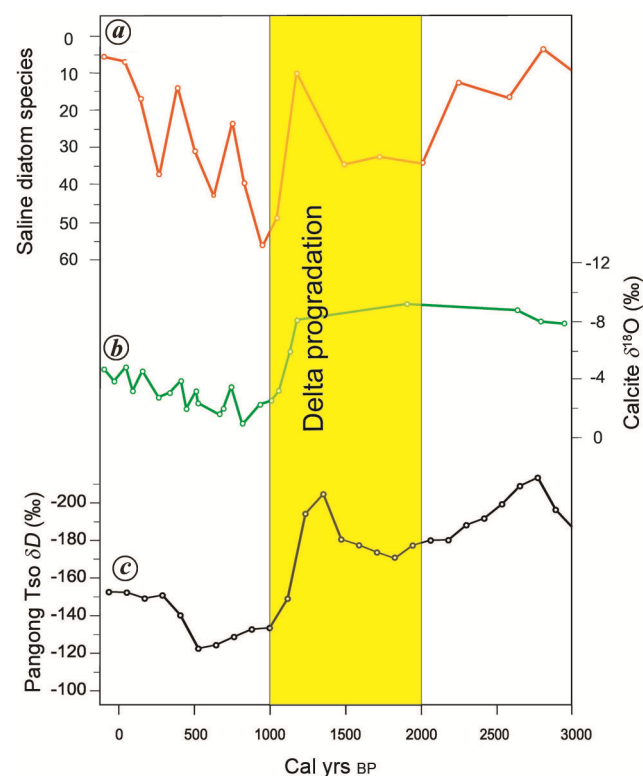


**Figure 7.** Lake level fall (this study) and climate proxy record from eastern Pangong Tso<sup>58</sup>. Trend of (a) salinity loving diatom species, (b)  $\delta^{18}\text{O}$  of lake calcite and (c)  $\delta\text{D}$  derived from leaf wax of Pangong Tso sediments over the past 2 ka.

In shell A, this inference can be best observed, possibly indicating that the shell analysed had completed its life cycle (Figure 6a). Shell B does not exhibit two perfect troughs, but the pattern remains similar, possibly due to the smaller size of the shell. In shell C, again a complete pattern is not obtained, and also there is an inverse correlation between  $\delta^{18}\text{O}$  and  $\delta^{13}\text{C}$  values during the inferred ISM season, indicating an anomalous input of carbon from an external source, such as a landslide into the lake. Thus, since sampling was done in a way which reflects the trend of the annual precipitation cycle and this trend was inferred to be comparable with present day annual precipitation trends. This comparison shows the relatively wider extent (months) of both the ISM and westerly precipitation in the time during which the shell lived, i.e. ~1.6 ka. This also falls in line with the  $\delta^{13}\text{C}$  values, which show a parallel trend, where the higher uptake of the lighter isotope by phytoplanktons in the lake during the dry period is reflected by a high point in the curve. This period also coincided with the phase of enriched  $\delta^{18}\text{O}$  values. This highlights the fact that biological productivity possibly had an inverse relationship with precipitation.

Using a wider extent of sampling area for shells, and collecting living specimens to perform sclerochronological analysis, could potentially provide a more comprehensive set of data and give a well-supported insight into the precipitation and temperature regime from 1.6 ka. Thus, short-term as well as long-term fluctuations in the ISM and westerly precipitation systems, as well as present day isotopic composition of these waters (from GNIP data) are needed to be studied in detail. This would allow us to understand the present day climate as well as enhance future hydrodynamic potential of the TP, which is an area in dire need of conservation of its people and environment, being ceremoniously known as the 'Water towers of the world', housing indigenous people and being an exotic biodiversity hotspot of our country as well as the world.

- Cohen, A. S., *Paleolimnology: the History and Evolution of Lake Systems*, Oxford University Press, 2003.
- Coulthard, T. J., Lewin, J. and Macklin, M. G., Modelling differential catchment response to environmental change. *Geomorphology*, 2005, **69**(1–4), 222–241.
- Dietze, E. et al., Basin morphology and seismic stratigraphy of Lake DonggiCona, north-eastern Tibetan Plateau, China. *Quaternary Int.*, 2010, **218**(1–2), 31–142.
- Zhang, Y., Wünnemann, B., Bezrukova, E. V., Ivanov, E. V., Shchetnikov, A. A., Nourgaliev, D. and Levina, O. V., Basin morphology and seismic stratigraphy of Lake Kotokel, Baikal region, Russia. *Quaternary Int.*, 2013, **290**, 57–67.
- Ghimire, S. and Higaki, D., Dynamic river morphology due to land use change and erosion mitigation measures in a degrading catchment in the Siwalik Hills, Nepal. *Int. J. River Basin Manage.*, 2015, **13**(1), 27–39.
- Ma, R. et al., China's lakes at present: number, area and spatial distribution. *Sci. China Earth Sci.*, 2011, **54**(2), 283–289.
- Negi, S. S., *Cold Deserts of India*, Indus Publishing, New Delhi, 2002, 2nd edn, p. 248.
- Bhat, F. A., Yousuf, A. R., Aftab, A., Arshid, J., Mahdi, M. D. and Balkhi, M. H., Ecology and Biodiversity in Pangong Tso (lake) and Its Inlet Stream in Ladakh, India. *Int. J. Biodivers. Conserv.*, 2011, **3**, 501–511.
- Chang, W. Y., Large lakes of China. *J. Great Lakes Res.*, 1987, **13**(3), 235–249.
- Boominathan, M. and Ramachandra, T. V., Molluscs of Pangong Tso, a high altitude brackish water lake in Ladakh, 2010.
- Klimes, L., Life-forms and clonality of vascular plants along an altitudinal gradient in E Ladakh (NW Himalayas). *Basic Appl. Ecol.*, 2003, **4**(4), 317–328.
- Bookhagen, B., Thiede, R. C. and Strecker, M. R., Late Quaternary intensified monsoon phases control landscape evolution in the northwest Himalaya. *Geology*, 2005, **33**(2), 149–152.
- Weiers, S., ZurKlimatologie des NW Karakoram und AngrenzenderGebiete. *Bonner Geogr. Abh.*, Bonn, Germany, 1994, p. 169.
- Staubwasser, M. and Weiss, H., Holocene climate and cultural evolution in late prehistoric–early historic West Asia. *Quaternary Res.*, 2006, **66**(3), 372–387.
- Government of Jammu and Kashmir, Environment and social management framework for Participatory Watershed Management Project (PWMP) J&K, IWDP-Hills II, 2007, Annex, p. 130.
- Hartmann, H., Zur Flora und Vegetation der Halbwüsten, Steppen und Rasengesellschaften im südöstlichen Ladakh (Indien). *Jahrbuch des Vereins zum Schutz der Bergwelt*, 1997, **62**, 129–188.
- Hartmann, H., Studien zur Flora und Vegetation im östlichen Transhimalaya von Ladakh (Indien). *Candollea*, 1999, **54**, 171–230.
- Pant, R. K., Phadtare, N. R., Chamyal, L. S. and Juyal, N., Quaternary deposits in Ladakh and Karakoram Himalaya: a treasure trove of the palaeoclimate records. *Curr. Sci.*, 2005, **88**(11), 1789–1798.
- Trinkler, E., The ice-age on the Tibetan Plateau and in the adjacent regions. *Geographical J.*, 1930, **75**(3), 225–232.
- Srikantia, S. V., Ganesan, T. M. and Wangdus, C., A note on the tectonic framework and geologic set-up of the Pangong–Chushul sector, Ladakh Himalaya. *J. Geol. Soc. India*, 1982, **23**(7), 354–357.
- Jain, A. K. and Singh, S., Tectonics of the southern Asian Plate margin along the Karakoram Shear Zone: constraints from field observations and U–Pb SHRIMP ages. *Tectonophysics*, 2008, **451**(1–4), 186–205.
- Srivastava, P., Brook, G. A., Marais, E., Morthekai, P. and Singhvi, A. K., Depositional environment and OSL chronology of the Homeb silt deposits, Kuiseb River, Namibia. *Quaternary Res.*, 2006, **65**(3), 478–491.
- Srivastava, P., Tripathi, J. K., Islam, R. and Jaiswal, M. K., Fashion and phases of late Pleistocene aggradation and incision in the Alaknanda River Valley, western Himalaya, India. *Quaternary Res.*, 2008, **70**(1), 68–80.
- Murray, A. S. and Wintle, A. G., Luminescence dating of quartz using an improved single-aliquot regenerative-dose protocol. *Radiat. Measur.*, 2000, **32**(1), 57–73.
- Aitken, M. J., Introduction to optical dating: the dating of Quaternary sediments by the use of photon-stimulated luminescence, Clarendon Press, 1998.
- Prescott, J. R. and Stephan, L. G., The contribution of cosmic radiation to the environmental dose for thermoluminescence dating. Latitude, altitude and depth dependences. *PACT*, 1982, **6**, 17–25.
- Gupta, S. K. and Polach, H. A., *Radiocarbon Dating Practices at ANU*, 1985.
- Stuiver, M. and Reimer, P. J., Extended  $^{14}\text{C}$  data base and revised CALIB 3.0  $^{14}\text{C}$  age calibration program. *Radiocarbon*, 1993, **35**(1), 215–230.
- Anderson, R., An annotated list of the non-marine Mollusca of Britain and Ireland. *J. Conchol.*, 2005, **38**(6), 607–638.
- Hutchinson, G. E., Limnological studies in Indian Tibet. *Int. Hydrobiol.*, 1937, **35**, 134–177.
- Brown, E. T., Bendick, R., Bourles, D. L., Gaur, V., Molnar, P., Raisbeck, G. M. and Yiou, F., Early Holocene climate recorded

- in geomorphological features in Western Tibet. *Palaeogeogr., Palaeoclimatol., Palaeoecol.*, 2003, **199**(1–2), 141–151.
32. Ou, Y. X. and Liu, D. S., Hydrologic characteristics of the east Bangong Lake. In *Geological and Ecological Studies of Qinghai-Xizang Plateau*. Proceedings of Symposium on Qinghai-Xizang (Tibet) Plateau, Beijing, China, Science Press and Gordon and Breach, Beijing, 1981, pp. 1713–1717.
  33. Drew, F., Alluvial and lacustrine deposits and glacial records of the Upper-Indus Basin. *Quarterly J. Geol. Soc.*, 1873, **29**(1–2), 441–471.
  34. Fontes, J. C., Gasse, F. and Gibert, E., Holocene environmental changes in Lake Bangong basin (Western Tibet). Part 1: chronology and stable isotopes of carbonates of a Holocene lacustrine core. *Palaeogeogr., Palaeoclimatol., Palaeoecol.*, 1996, **120**(1–2), 25–47.
  35. Huang, C. X., A preliminary study of paleovegetation and paleoclimate in the later period of late Pleistocene in Bangongcuo Lake region of Xizang. *J. Nat. Res.*, 1989, **4**, 247–253.
  36. Shi, Y., Yu, G., Liu, X., Li, B. and Yao, T., Reconstruction of the 30–40 ka BP enhanced Indian monsoon climate based on geological records from the Tibetan Plateau. *Palaeogeogr., Palaeoclimatol., Palaeoecol.*, 2001, **169**(1–2), 69–83.
  37. Nemecek, W., Aspects of sediment movement on steep delta slopes. In *Coarse-Grained Deltas*, 1990, vol. 10, pp. 29–73.
  38. Bristow, C. S., Holmes, J. A., Matthey, D., Salzmann, U. and Sloane, H. J., A late Holocene palaeoenvironmental ‘snapshot’ of the Angamma Delta, Lake Megachad at the end of the African Humid Period. *Quaternary Sci. Rev.*, 2018, **202**, 182–196.
  39. Mordan, P. and Wade, C., Heterobranchia-II. *Phylogeny and Evolution of the Mollusca*, 2008, p. 409.
  40. Röpstorf, P. and Riedel, F., Deep-water gastropods endemic to Lake Baikal – an SEM study on protoconchs and radulae. *J. Conchology*, 2004, **38**, 253.
  41. Taft, L., Wiechert, U., Riedel, F., Weynell, M. and Zhang, H., Sub-seasonal oxygen and carbon isotope variations in shells of modern *Radix* sp. (Gastropoda) from the Tibetan Plateau: potential of a new archive for palaeoclimatic studies. *Quaternary Sci. Rev.*, 2012, **34**, 44–56.
  42. Gaten, E., Life cycle of *Lymnaea peregra* (Gastropoda: Pulmonata) in the Leicester canal, UK, with an estimate of annual production. *Hydrobiologia*, 1986, **135**(1–2), 45–54.
  43. Huntington, E., Pangong: a glacial lake in the Tibetan Plateau. *J. Geol.*, 1906, **14**(7), 599–617.
  44. Philip, G. and Mazari, R. K., Shrinking lake basins in the proximity of the Indus Suture Zone of northwestern Himalaya: a case study of Tso Kar and Startsapuk Tso, using IRS-1C data. *Int. J. Remote Sensing*, 2000, **21**, 2973–2984.
  45. Sangode, S. J., Meshram, D. C., Rawat, S., Suresh, N. and Srivastava, P., Sedimentary and geomorphic observations along Pangong strand of the Karakorum Fault (NW Himalaya) depicting Holocene Uplift. *Himalayan Geol.*, 2017, **38**(2), 111–128.
  46. Walker, M. J. *et al.*, Formal subdivision of the Holocene Series/Epoch: a discussion paper by a working group of INTIMATE (Integration of ice-core, marine and terrestrial records) and the subcommission on quaternary stratigraphy (International Commission on Stratigraphy). *J. Quaternary Sci.*, 2012, **27**(7), 649–659.
  47. Rawat, S., Gupta, A. K., Sangode, S. J., Srivastava, P. and Nainwal, H. C., Late Pleistocene–Holocene vegetation and Indian summer monsoon record from the Lahaul, northwest Himalaya, India. *Quaternary Sci. Rev.*, 2015, **114**, 167–181.
  48. Owen, L. A., Latest Pleistocene and Holocene glacier fluctuations in the Himalaya and Tibet. *Quaternary Sci. Rev.*, 2009, **28**(21–22), 2150–2164.
  49. Mehta, M., Majeed, Z., Dobhal, D. P. and Srivastava, P., Geomorphological evidences of post-LGM glacial advancements in the Himalaya: a study from Chorabari Glacier, Garhwal Himalaya, India. *J. Earth Syst. Sci.*, 2012, **121**(1), 149–163.
  50. Mehta, M., Dobhal, D. P., Pratap, B., Majeed, Z., Gupta, A. K. and Srivastava, P., Late quaternary glacial advances in the tons river valley, Garhwal Himalaya, India and regional synchronicity. *The Holocene*, 2014, **24**(10), 1336–1350.
  51. Shukla, T., Mehta, M., Jaiswal, M. K., Srivastava, P., Dobhal, D. P., Nainwal, H. C. and Singh, A. K., Late Quaternary glaciation history of monsoon-dominated Dingad basin, central Himalaya, India. *Quaternary Sci. Rev.*, 2018, **181**, 43–64.
  52. Kumar, A., Srivastava, P. and Meena, N. K., Late Pleistocene aeolian activity in the cold desert of Ladakh: a record from sand ramps. *Quaternary Int.*, 2017, **443**, 13–28.
  53. Srivastava, P. *et al.*, Paleofloods records in Himalaya. *Geomorphology*, 2017, **284**, 17–30.
  54. Demske, D., Tarasov, P. E., Wünnemann, B. and Riedel, F., Late glacial and Holocene vegetation, Indian monsoon and westerly circulation in the Trans-Himalaya recorded in the lacustrine pollen sequence from Tso Kar, Ladakh, NW India. *Palaeogeogr., Palaeoclimatol., Palaeoecol.*, 2009, **279**(3), 172–185.
  55. Leipe, C., Demske, D., Tarasov, P. E., Wünnemann, B., Riedel, F. and Members, H. P., Potential of pollen and non-pollen palynomorph records from TsoMoriri (Trans-Himalaya, NW India) for reconstructing Holocene limnology and human–environmental interactions. *Quaternary Int.*, 2014, **348**, 113–129.
  56. Mishra, P. K. *et al.*, Carbonate isotopes from high altitude TsoMoriri Lake (NW Himalayas) provide clues to late glacial and Holocene moisture source and atmospheric circulation changes. *Palaeogeogr., Palaeoclimatol., Palaeoecol.*, 2015, **425**, 76–83.
  57. Wünnemann, B. *et al.*, Hydrological evolution during the last 15 kyr in the Tso Kar lake basin (Ladakh, India), derived from geomorphological, sedimentological and palynological records. *Quaternary Sci. Rev.*, 2010, **29**(9–10), 1138–1155.
  58. Phartiyal, B., Singh, R. and Kothyari, G. C., Late-quaternary geomorphic scenario due to changing depositional regimes in the Tangtse Valley, Trans-Himalaya, NW India. *Palaeogeogr., Palaeoclimatol., Palaeoecol.*, 2015, **422**, 11–24.
  59. Dortch, J. M., Owen, L. A., Caffee, M. W. and Kamp, U., Catastrophic partial drainage of Pangong Tso, northern India and Tibet. *Geomorphology*, 2011, **125**(1), 109–121.
  60. Hou, J., D’Andrea, W. J., Wang, M., He, Y. and Liang, J., Influence of the Indian monsoon and the subtropical jet on climate change on the Tibetan Plateau since the late Pleistocene. *Quaternary Sci. Rev.*, 2017, **163**, 84–94.
  61. Mishra, P. K. *et al.*, Reconstructed late quaternary hydrological changes from Lake TsoMoriri, NW Himalaya. *Quaternary Int.*, 2015, **371**, 76–86.
  62. Dutt, S., Gupta, A. K., Wünnemann, B. and Yan, D., A long arid interlude in the Indian summer monsoon during? 4350 to 3450 cal. yr BP contemporaneous to displacement of the Indus valley civilization. *Quaternary Int.*, 2018, **482**, 83–92.
  63. Chakraborty, S., Bhattacharya, S. K., Ranhotra, P. S., Bhattacharyya, A. and Bhushan, R., Palaeoclimatic scenario during Holocene around Sangla valley, Kinnaur northwest Himalaya based on multi proxy records. *Curr. Sci.*, 2006, **91**(6), 777–782.
  64. Yadav, R. R., Gupta, A. K., Kotlia, B. S., Singh, V., Misra, K. G., Yadava, A. K. and Singh, A. K., Recent wetting and glacier expansion in the northwest Himalaya and Karakoram. *Sci. Rep.*, 2017, **7**(1), 6139.

ACKNOWLEDGEMENTS. We acknowledge the Directors of our respective organizations for providing support. Field mapping was done during a field training course funded by Department of Science and Technology, New Delhi via grant Project# SR/FTP/ES-41/2012. Wild Life Authorities and DC, Leh are acknowledged for extending necessary permissions to work in the area. Dr Navin Juyal is acknowledged for helping in the field.

doi: 10.18520/cs/v119/i2/219-231